Nanoscale Structural and Chemical Properties of Antipolar Clusters in Sm-Doped BiFeO$_3$ Ferroelectric Epitaxial Thin Films

Ching-Jung Cheng,*,[†] Albina Y. Borisevich,*,[‡] Daisuke Kan,[§] Ichiro Takeuchi,[§] and Valanoor Nagarajan*,[†]

[†]*School of Materials Science and Engineering, University of New South Wales, New South Wales 2052, Australia,* [‡]*Materials Science and Technology Division, Oak Ridge National Laboratory, Oak Ridge, Tennessee 37831, and* [§]*Department of Materials Science and Engineering, University of Maryland, College Park, Maryland 20742*

The local atomic structure and nanoscale chemistry of an antipolar phase in Bi$_{0.9}$Sm$_{0.1}$FeO$_3$ epitaxial thin films are examined by an array of transmission electron microscopy (TEM) coupled with electron diffraction and electron energy-loss spectroscopy methods. The observations are tied to macroscopic properties of the films, namely, polarization-electric field hysteresis loops, dielectric constant-electric field hysteresis loops, and the dielectric loss. At room temperature, the local Sm deficiency was determined to destabilize the long-range ferroelectric state, resulting in the formation of local antipolar clusters with the appearance of PbZrO$_3$-like antiparallel cation displacements, which give rise to $^1/_4${011} and $^1/_4${211} reflections as well as $^1/_2${321}, because of in-phase oxygen octahedral tilts. Aberration-corrected TEM analysis reveals that the antipolar structure is actually a lamellar of highly dense ferroelectric domains with alternating polarizations. With increasing temperature, a phase transition was observed at 150 °C, which is attributed to the reduction of the antiparallel displacements, giving way to cell-doubling structural transition.

I. Introduction

Bismuth ferrite (or BiFeO$_3$, BFO) is one of the most extensively studied multiferroic materials with two robust ferroic phase transitions well above room temperature (i.e., 370 °C for the antiferromagnetic Neel temperature and 830 °C for the ferroelectric (FE) Curie temperature).[1,2] BFO has a rhombohedral distorted ABO$_3$ perovskite-type oxide structure (where A and B are cations), with space group $R3c$, which allows antiphase oxygen octahedral tilts and cation displacements from the centro-symmetric positions along the [111] pseudo-cubic direction.[3,4] Although BFO has been identified as a possible environmentally friendly alternative to current lead lead-based piezoelectrics, it suffers from high-leakage current and large coercive fields, as well as electromechanical coefficients much smaller than traditional lead-based compositions. It has been shown that some of the aforementioned shortcomings can be overcome by cation doping of the

BFO perovskite cell.[5−7] The rationale behind such doping experiments is the fact that the subtle changes in atomic composition can induce distortion of the perovskite cell and, hence, create phase transitions that may lead to new and improved functional properties.[5,6,8,9]

For example, it has been shown in several reports that doped BFO leads to slight deviations from the ideal perovskite (aristotype) structure, because of mechanisms such as reduction of tetragonality,[5,7] rotation of oxygen octahedral,[10,11] cation ordering,[12,13] and/or cation displacements.[10,11] The observed systematic links between the variations of the structure of ferroelectric BFO (as a function of varying composition, temperature, applied stress, etc.) and the measured physical properties have been attributed to an intimate interplay between variations

*Author to whom correspondence should be addressed. E-Mail: nagarajan@unsw.edu.au.

(1) Wang, J.; Neaton, J. B.; Zheng, H.; Nagarajan, V.; Ogale, S. B.; Liu, B.; Viehland, D.; Vaithyanathan, V.; Schlom, D. G.; Waghmare, U. V.; Spaldin, N. A.; Rabe, K. M.; Wuttig, M.; Ramesh, R. *Science* **2003,** *299,* 1719.
(2) Selbach, S. M.; Tybell, T.; Einarsrud, M. A.; Grande, T. *Adv. Mater.* **2008,** *20,* 3692.
(3) Ederer, C.; Spaldin, N. A. *Phys. Rev. B* **2005,** *71,* 060401.
(4) Woodward, D. I.; Reaney, I. M. *Acta Crystallogr., Sect. B: Struct. Sci.* **2005,** *B61,* 387.
(5) Chu, Y. H.; Zhan, Q.; Yang, C. H.; Cruz, M. P.; Martin, L. W.; Zhao, T.; Yu, P.; Ramesh, R.; Joseph, P. T.; Lin, I. N.; Tian, W.; Schlom, D. G. *Appl. Phys. Lett.* **2008,** *92,* 102909.

(6) Yuan, G. L.; Or, S. W. *J. Appl. Phys.* **2006,** *100,* 024109.
(7) Uchida, H.; Ueno, R.; Funakubo, H.; Koda, S. *J. Appl. Phys.* **2006,** *100,* 014106.
(8) Fujino, S.; Murakami, M.; Anbusathaiah, V.; Lim, S. H.; Nagarajan, V.; Fennie, C. J.; Wuttig, M.; Salamanca-Riba, L.; Takeuchi, I. *Appl. Phys. Lett.* **2008,** *92,* 202904.
(9) Selbach, S. M.; Tybell, T.; Einarsrud, M. A.; Grande, T. *Chem. Mater.* **2009,** *21,* 5176.
(10) Cheng, C. J.; Kan, D.; Lim, S. H.; McKenzie, W. R.; Munroe, P. R.; Salamanca-Riba, L. G.; Withers, R. L.; Takeuchi, I.; Nagarajan, V. *Phys. Rev. B* **2009,** *80,* 014109.
(11) Karimi, S.; Reaney, I. M.; Levin, I.; Sterianou, I. *Appl. Phys. Lett.* **2009,** *94,* 112903.
(12) Yang, C. H.; Seidel, J.; Kim, S. Y.; Rossen, P. B.; Yu, P.; Gajek, M.; Chu, Y. H.; Martin, L. W.; Holcomb, M. B.; He, Q.; Maksymovych, P.; Balke, N.; Kalinin, S. V.; Baddorf, A. P.; Basu, S. R.; Scullin, M. L.; Ramesh, R. *Nature Mater.* **2009,** *8,* 485.
(13) Schiemer, J.; Withers, R.; Noren, L.; Liu, Y.; Bourgeois, L.; Stewart, G. *Chem. Mater.* **2009,** *21,* 4223.

in the polar order and the crystal structure of the material. We previously reported that the *A*-site substitution of the perovskite BFO with Sm^{3+} ions results in a structural transition from the rhombohedral phase to an orthorhombic phase where double hysteresis loops (in polarization-electric field loops) are observed, accompanied by a substantial enhancement of the electromechanical properties at the phase boundary.[8] In the following study, it was shown that the structural transition and enhanced properties can occur, independent of the rare-earth (RE) dopant species; furthermore, it can be universally achieved by controlling the average ionic radius of the *A*-site cation.[14] In the same study, we also showed that the same phase transitions and the atomic-structure changes occur, irrespective of the substrates. We have used the first-principles calculations to explore the energy landscape of BFO and proposed that the origin of the double hysteresis loop and the concomitant enhancement in the piezoelectric coefficient is an electric-field-induced transformation from a paraelectric (PE) orthorhombic phase to the polar rhombohedral phase at the boundary.[14]

Karimi et al. showed that RE^{3+} doping of the BFO within a critical composition range affects short-range antiparallel (sideways) interactions between the cations, leading to formation of antipolar $PbZrO_3$ (PZO)-like clusters (evidenced by observation of local commensurate $^1/_4\{011\}$ reflections).[15] It has been demonstrated that these antipolar clusters then grow within a FE matrix with increasing RE^{3+} content and at a critical concentration where FE regions are so frustrated by the surrounding antipolar matrix, it results in an incommensuration phenomenon where the system adopts a complex nanoscale mixture bridging between bismuth-rich rhombohedral and RE-rich orthorhombic phases.[10]

While such studies have helped to delineate the main features of structural evolution in RE-doped BFO, to date, there is very little information on the atomic-level (i.e., local) chemical origins of the nascent antipolar cluster states. Understanding the origins of these clusters is critical, because it is these local clusters that are the first visible signatures of order frustration, which ultimately leads to the structural phase transition.[14,15] Further information on the precise chemical environments of these clusters can help identify solid-state chemistry routes to artificially induced phase transformations potentially common to a wide range of ferroelectric piezoelectric materials.

The focus of this study thus is to elucidate the important features of the antipolar clusters at atomic scale and link their local chemical and structural properties to the observed functional properties. We examined 10%-Sm-doped BFO (which is a composition known to display antipolar clusters[10]) with an array of transmission electron microscopy (TEM) techniques, namely, high-resolution transmission electron microscopy (HRTEM) coupled with selected-area electron diffraction (SAED) analysis, aberration-corrected scanning transmission electron microscopy (STEM), and spatially resolved electron energy-loss spectroscopy (EELS) to determine the underpinning structural features of the antipolar clusters. The structural origins are ultimately linked to the observed ferroelectric properties characterized via polarization−electric field ($P-E$) hysteresis loops, dielectric constant−electric field ($\varepsilon_{33}-E$) hysteresis loops, and dielectric loss ($\tan\delta$) measured as a function of temperature.

We demonstrate that the antipolar clusters in the Sm-doped BFO system are a consequence of a destabilized zone center FE polar state. Aberration-corrected STEM images show direct evidence of the antipolar displacement order and EELS data reveal significant changes in the samarium chemistry for the clusters, in contrast to the surrounding FE matrix. Diffraction studies reveal that the antipolar clusters may have different orientational displacement variants (i.e., structural twins) coupled with in-phase oxygen octahedral tilts. At higher temperatures, cation interactions become much weaker and in favor of the unit-cell-doubled orthorhombic phase, which is a similar analogy to the observed room-temperature structural transitions for higher Sm^{3+} content.[10]

II. Experimental Section

10%-Sm-doped $BiFeO_3$ ($Bi_{0.9}Sm_{0.1}FeO_3$) epitaxial thin films (200 nm thick, (001)-oriented) were fabricated on a $SrTiO_3$ (001) substrate with a $SrRuO_3$ electrode (50 nm) as a buffer layer by pulsed laser deposition with a KrF laser. The exact composition was confirmed by electron probe microanalyzer (JEOL, Model JXA 8900). We choose 10% Sm-doped BFO as our composition of interest, because we have previously seen clear and visible clusters with PZO-like features surrounded by the aristotype FE matrix to be formed in this material.[10]

The cross-sectional TEM specimens were prepared by the standard tripod wedge polishing technique followed by argon ion thinning at 3 kV by PIPS (Gatan, Model 691) to electron transparency. The specimen is then transferred to a GentleMill apparatus (Technoorg Linda, IV5) for final polishing on both sides at 0.6 kV for 1 h, to clean any surface artifacts before TEM examination. All HRTEM and SAED work was obtained using a JEOL Model 3000F TEM operating at 300 kV with a double-tilt holder to obtain different zone axes. All electron diffraction patterns used here are indexed as pseudo-cubic unit-cell notation.

STEM and EELS work was conducted on an FEI Titan aberration-corrected microscope operated at 300 kV and equipped with a dodecapole corrector (CEOS GmbH) for the electron probe, as well as a GIF 2001 post-column imaging filter. The probe convergence semiangle was 27.5 mrad, the inner detector semiangle used for high-angle annular dark-field (HAADF) imaging was 80 mrad, and the EELS collection semiangle was 10 mrad. The spectra were recorded with 1 eV dispersion and collection times up to 30 s.

(14) Kan, D.; Palova, L.; Anbusathaiah, V.; Cheng, C. J.; Fujino, S.; Nagarajan, V.; Rabe, K. M.; Takeuchi, I. *Adv. Funct. Mater.* In press.

(15) Karimi, S.; Reaney, I. M.; Han, Y.; Pokorny, J.; Sterianou, I. *J. Mater. Sci.* **2009**, *44*, 5102.

(a)

(b)   **(c)**
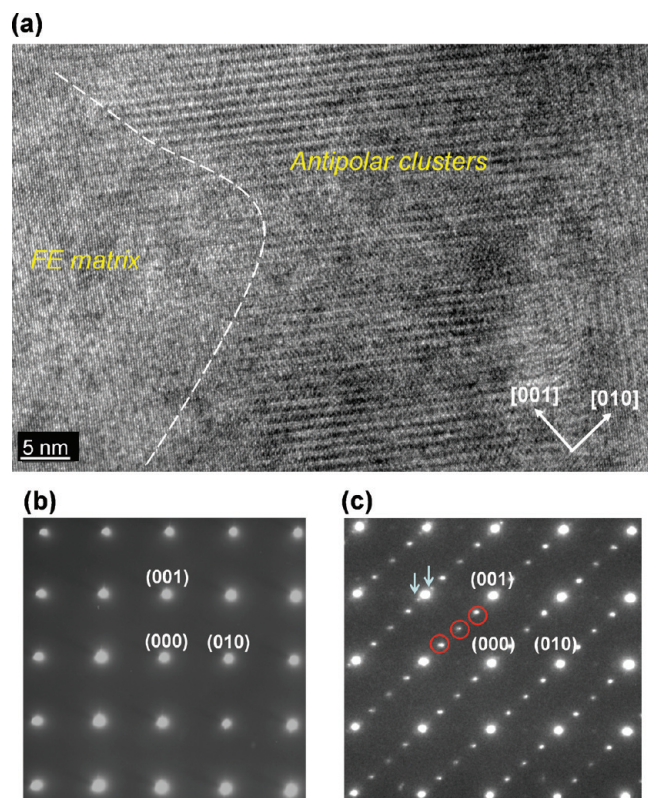
Figure 1. (a) Cross-sectional HRTEM image of $Bi_{0.9}Sm_{0.1}FeO_3$ thin film along the [100] zone axis, showing the continuous interface between an antipolar cluster and the FE matrix, indicated by the dashed lines (used as an approximate guide to the eye); arrows indicate the [001] and [010] zone axes. (b) [100] ZADP from the FE matrix, indicating fundamental reflections. (c) [100] ZADP from antipolar cluster; the circled features denote $^1/_4\{011\}$ reflections due to antiparallel cation displacements, and the arrowed spots come from interfacially modulated incommensuration.

Temperature-dependent studies on $P-E$ hysteresis loops were obtained at a frequency of 25 kHz using a Radiant Premiere II analyzer, dielectric constant−electric field ($\varepsilon_{33}-E$) hysteresis loops and dielectric loss (tan δ) measurements were acquired using a Hewlett Packard Model HP 4275A LCR meter at 100 kHz. The high-temperature X-ray experiment was performed by a two-dimensional X-ray diffraction (XRD) system (Bruker D8 with a Hi-Star detector).

III. Results and Discussion

High-Resolution TEM Studies. Recently, we had reported a low-magnification bright-field cross-sectional TEM image of $Bi_{0.9}Sm_{0.1}FeO_3$ thin film, which revealed the existence of local clusters $\sim10-20$ nm in size.[10] These pockets showed the distinct appearance of $^1/_4\{011\}$ super-structure spots, in addition to the fundamental perovskite reflections. The clusters begin to appear at a samarium doping of $\sim8\%$[14] and, with increasing samarium content, begin to grow.[10] As a consequence of these local antipolar clusters, complex instabilities within the perovskite framework are expected. We begin with HRTEM investigations of these clusters, with particular emphasis on the interface between the FE matrix and the antipolar cluster indicated by the dashed line in Figure 1a, which shows such a cross-sectional HRTEM image at the [100] zone

axis of the $Bi_{0.9}Sm_{0.1}FeO_3$ thin film, with clear indication of a two-phase mixture. The [100] zone axis diffraction patterns (ZADP) of the FE matrix phase and the cluster are shown in Figures 1b and 1c, respectively. The diffraction pattern shown in Figure 1c has been previously observed in the room-temperature orthorhombic phase in PZO and understood as a result of softening of the Σ_3 mode containing antiparallel Pb alignment of dipole moments along the $\langle011\rangle$ axis. This gives rise to the orthorhombic antiferroelectric (AFE) state in PZO, indicated by $^1/_4\{011\}$ reflections in a typical PZO electron diffraction pattern.[16,17] Thus, the circled $^1/_4\{011\}$ commensurate ordering in Figure 1c results from dipoles equally displaced, but in opposite directions, with antiparallel arrangements. This produces a quadrupling of the unit cell along the $\langle011\rangle$ direction with dimensions of $\sqrt{2}a \times 2\sqrt{2}a \times 2a$, where a is the lattice parameter of the pseudo-cubic perovskite unit cell.[17] Furthermore, the diffraction pattern of the clusters contain arrowed local $(1/x)\{011\}$ incommensurate reflections. We do not believe epitaxial strain is playing a significant role in the occurrence of the phenomena reported here. We have previously reported that the films on STO are almost entirely or at least partially relaxed,[8] We have also demonstrated that Sm-substituted BFO films 400 nm thick, grown on different substrates with different lattice parameters (LSAT $((LaAlO_3)_{0.3}-(SrAl_{0.5}Ta_{0.5}O_3)0.7)$, STO, and $DyScO_3$) reproduce the same structural and ferroelectric behaviors as those of 200-nm -thick Sm-BFO films on STO.[14]

Careful examination of the HRTEM image in Figure 1a reveals that the interface marked with the dashed line (which is present as a guide) has several regions where slabs of the antipolar quadrupled unit cells coalesce with FE (cubic aristotype unit cells) phases. These lead to *interfacially* modulated incommensuration, which is a consequence of superposition of cation displacements across two regions. (The detailed aberration-corrected HRTEM of the interface is given in Figure 6a, presented later in this paper.) The interfacially incommensurable character generally occurs when the dimension of one modulation does not fit into another underlying modulation, because of a different coupling constant; hence, it gives rise to $(1/x)\{011\}$ reflections as a bridging phase.[18] The supercell formed as a result of the antipolar clusters is schematically illustrated in Figure 2a in real space with a pseudo-cubic symmetry. The black lines represent fundamental unit cells, whereas the red unit cell illustrates the supercell formed because of the antiparallel A-site displacements along the [011] direction. Figure 2b shows a polyhedral illustration of a perovskite network showing both an antiparallel shift in A-site cations (indicated by arrows) and distortion of oxygen octahedra. This shows how the displacement ordering

(16) Viehland, D. *Phys. Rev. B* **1995**, *52*, 778.
(17) Woodward, D. I.; Knudsen, J.; Reaney, I. M. *Phys. Rev. B* **2005**, *72*, 104110.
(18) Viehland, D.; Dai, X. H.; Li, J. F.; Xu, Z. *J. Appl. Phys.* **1998**, *84*, 458.

Article

Chem. Mater., Vol. 22, No. 8, 2010 2591
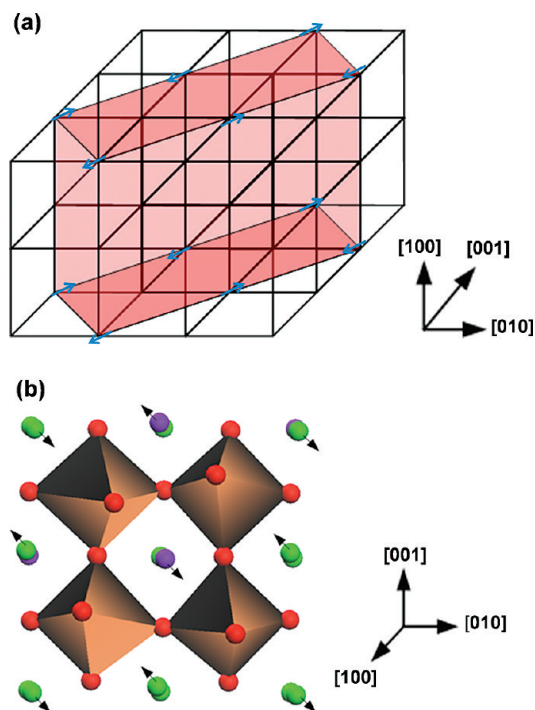
Figure 2. (a) Schematic illustration in real space showing the red super-cell, which is formed along the [011] direction, as a result of the cation displacements (indicated by arrows) in the antipolar clusters. The black lines indicate the fundamental perovskite unit cells. The [001] direction corresponds to the out-of-plane direction of the film. (b) Polyhedral illustration of the perovskite network of antipolar cluster displaying both an antiparallel shift in *A*-site cations (indicated by arrows) coupled with distortion of oxygen octahedra. The green (and purple) balls represent Bi (and Sm) atoms. The brown octahedra with the red balls (O) in the corners represent FeO_6 octahedra.

along any of the ⟨011⟩ directions can give rise to the $^1/_4${011} ordered superstructure.

To further understand the structural features of the ordered regions in Figure 1, we focused on HRTEM and STEM investigations inside a representative cluster. Figure 3a is a cross-sectional HRTEM image that shows not only the ordering along the ⟨011⟩ directions but also a polydomain structure with a sharp twin boundary, which intersect to form right-angled domains (indicated by the dotted line). This is attributed to antipolar domain variants with *A*-site cations displaced in 90° crystallographic relations to each other. This particular pattern has been formerly observed at room temperature for PZO[16] when antiparallel cations shifts occur along both the [011] and [0$\bar{1}\bar{1}$] directions. Figure 3b is the [100] ZADP that captures the bidirectional antiparallel shift along {011} planes. This illustrates the close resemblance between the antipolar clusters seen here and the orthorhombic PZO, where the antipolar order is associated with a complex coupling between the Σ_3 mode and an oxygen rotation mode Γ_{25}, rather than arising from the two sublattice model, which involves the condensation of a single zone-boundary polar phonon mode.[16,19] Figure 3c is the aberration-corrected cross-sectional bright-field (BFSTEM) image of the same twin structure at the [100] zone axis. This image demonstrates the clear existence of a coherent
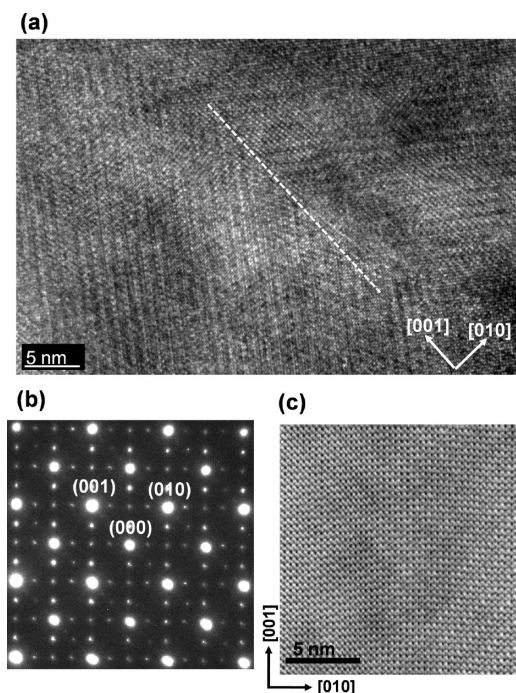
Figure 3. (a) [100] zone axis cross-sectional HRTEM image of a poly-domain structure inside clusters, with the twin wall indicated by the dotted line; (b) [100] ZADP showing bidirectional antiparallel shift along {011} planes; and (c) aberration-corrected bright-field image of the same twin structure with sharp interfaces.

nanoscale twin plane parallel to the [001] direction separating the $^1/_4$-related superstructure regions (the so-called ordered twin[20]), in good agreement with Figure 3a.

Twin structures generally occur as a result of an energy minimization process during a phase transformation. For instance, an ordered twinned structure has been previously observed at the morphotropic phase boundary (MPB) composition of 14% Sm-doped BFO.[10] However, the critical difference here is the distinct absence of $^1/_2${010} reflections, which have been shown to originate from an orthorhombic unit-cell doubling mechanism, coupled with antiphase octahedral tilts.[10] This shows that, at room temperature, for this 10% Sm-doped BFO composition, the orthorhombic unit-cell doubling mechanism is clearly missing and, hence, is not a necessary requirement for the onset of the antipolar cluster phase.

Aberration-Corrected *Z*-Contrast Imaging. Figure 4a is the [100] zone axis cross-sectional STEM bright field image of a region where domain boundaries of the $^1/_4$-related superstructure are marked by arrows. HAADF imaging or incoherent *Z*-contrast imaging was also performed with atomic column-by-column resolution to determine whether there is possible *A*-site cationic ordering in the antipolar clusters. Since, for a practical range of sample thicknesses, each bright spot in the image corresponds to exactly one atomic column in the sample and its intensity is approximately proportional to the atomic number Z^2 of the constituent atoms, this allows us to

(19) Cochran, W.; Zia, A. *Phys. Status Solidi* **1968**, *25*, 273.

(20) Lei, C. H.; Van Tendeloo, G.; Amelinckx, S. *Philos. Mag. A* **2002**, *82*, 349.

(a)

(b)

(c)

(d)
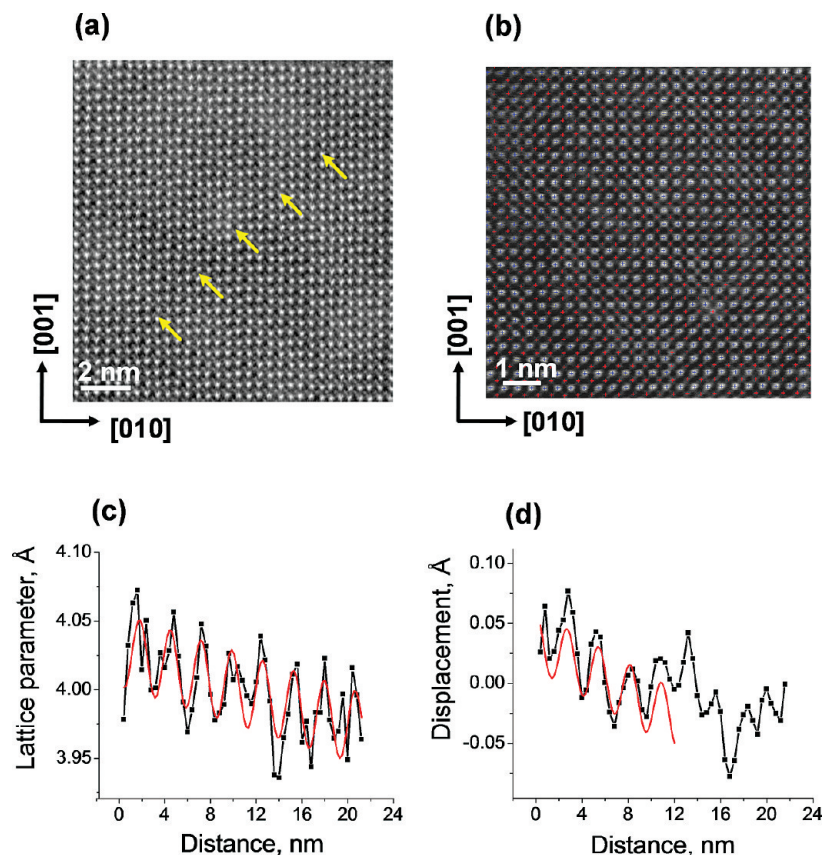
Figure 4. (a) [100] zone axis STEM bright field image. The $^1/_4$-related superstructure domain boundaries are marked by arrows; (b) aberration-corrected Z-contrast image of the anti-polar cluster signifying A-site chemical ordering is not taking place. This image was used to obtain atomic displacements of Bi (marked with blue plus markers) and Fe (marked with red plus markers) columns; (c) quantification of displacements of Bi atoms along the superstructure and (d) quantification of displacements of Fe atoms along the superstructure.

search for chemical origins of the ordered domains.[21−23] While our earlier results suggested that A-site chemical ordering is not a likely explanation for the superstructure spots,[10] this could not be verified directly, because of a lack of atomic-resolution data. In the present study, an aberration-corrected microscope with the atomic-scale spatial resolution gives us this opportunity for verification. From the [100] zone axis cross-sectional Z-contrast image in Figure 4a (domain boundaries of the $^1/_4$-related superstructure marked by arrows), it is clear that chemical ordering between Bi^{3+} and Sm^{3+} ions at atomic scale does not occur at all, because there is virtually no contrast difference between A-site atomic positions. Therefore, this provides direct evidence that the superstructure spots observed for the clusters originate from distortions to the parent lattice (either from cation displacements and/or oxygen octahedral rotation) rather than chemical ordering at the cationic sites of the perovskite cell.

Furthermore, we have quantified atomic displacements of the cations within the superstructure, as shown in the dark-field image shown in Figure 4b, which is a magnified

portion of Figure 4a with Bi columns marked with blue plus markers and Fe columns marked with red plus markers. For full details regarding the quantification procedure, the reader is referred to both files given in the Supporting Information. The resulting observed sets of atomic positions in the xy-plane are then used to obtain two-dimensional (2D) maps of lattice parameters (calculating difference in positions between neighboring Bi atoms) and cation displacements (Δx and Δy) (calculating the difference between the Fe position and the average of the neighboring Bi positions). Figure 4c plots the profile of the Bi−Bi distance (out-of-plane lattice parameter) along the superstructure direction, calculated from the full 2D map (details given in the Supporting Information). The profile exhibits modulation with a consistent periodicity, which is estimated as 2.745 ± 0.026 nm peak to peak. It is also notable that the sine fit underestimates the peak values of the modulation profile, which appears to be close to a zigzag. The profile of the Fe off-center displacement map taken in the same fashion across the superstructure is shown in Figure 4d, where the oscillations also appear consistent and visible. The sine fit on the entire range was not successful, because of the existence of an apparent stacking fault in the middle of the profile; however, the fit on half of the data yields a consistent periodicity value of 2.773 ± 0.064 nm peak to peak, suggesting that the lattice parameter modulation and the displacement modulation have the same origin. It is

(21) Sato, Y.; Mizoguchi, T.; Shibata, N.; Moriwake, H.; Hirayama, T.; Ikuhara, Y. *Appl. Phys. Lett.* **2009**, *95*, 022906.
(22) Yan, Y.; Pennycook, S. J.; Xu, Z.; Viehland, D. *Appl. Phys. Lett.* **1998**, *72*, 3145.
(23) Varela, M.; Lupini, A. R.; van Benthem, K.; Borisevich, A. Y.; Chisholm, M. F.; Shibata, N.; Abe, E.; Pennycook, S. J. *Annu. Rev. Mater. Res.* **2005**, *35*, 539.
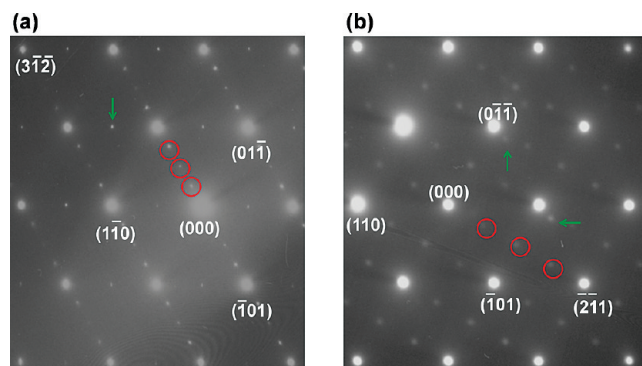
Figure 5. (a) [111] ZADP taken from antipolar cluster with circled $^1/_4\{011\}$ reflections due to antiparallel cation displacement as well as arrowed $^1/_2\{3\bar{1}2\}$ reflections coming from in-phase oxygen octahedral tilt and (b) [1$\bar{1}$1] ZADP of another cluster with appearance of circled $^1/_4\{\bar{2}11\}$ superstructure reflections. The arrowed weak spots possibly arise as a result of the structural deviations from the periodic lattice and lead to partial orderings.

especially noteworthy that, after a correction for sloping background likely arising from drift, the absolute values of the displacements change sign for every neighboring two-unit-cell domain, suggesting that the apparent antipolar order in this system is actually a lamellar array of highly dense ferroelectric domains with alternating polarizations.

We have conducted more tilting experiments focused on these clusters in Figure 5, with the intention to probe the nature of oxygen octahedra that forms the lattice. Figure 5a shows [111] ZADP with weak $^1/_4\{011\}$ superstructure reflections along the single direction of [$\bar{1}01$], as indicated by circles. This has been previously associated with antiparallel cation shifts. In addition, there are arrowed $^1/_2\{3\bar{1}2\}$ weak reflections occurring in more than one axis. We believe they are the results of in-phase oxygen octahedra tilts in more than one axis, as they satisfy the Glazer's selection rule of $^1/_2\{hk0\}$ (where $h \neq k$).[4,24] This in-phase ordering of oxygen octahedra does not occur unexpectedly, because RE orthoferrites such as $SmFeO_3$ contain mixed-tilt systems of both in-phase and antiphase octahedra rotation.[25,26] The Goldschmidt tolerance factor (t) predictions[17,27] for structures with decreasing t, the stability of perovskite network favors a mixed tilted perovskite of both in-phase and antiphase tilting of anion octahedra at room temperature (for the case of $Bi_{0.9}Sm_{0.1}FeO_3$; $t \approx 0.95$). This shows that, at 10% Sm-doped BFO, the system has already moved away from antiphase tilted rhombohedral BFO. In the case of Nd-substituted BFO ceramics, both in-phase octahedral tilts and cation displacement have also been observed,[11] which are akin to the $NaNbO_3$-type phase transition.[28]

Figure 5b shows the [1$\bar{1}$1] ZADP of another cluster on the film, where the appearance of $^1/_4\{\bar{2}11\}$ superstructure

reflections is circled. This is associated with anharmonic coupling between zone-boundary Σ_3 and Γ_{25} oxygen rotational modes, again a phenomenon that is known to be the primary mode that is stabilized in AFE Zr-rich $Pb(Zr,Ti)O_3$ and one that gives rise to $\langle ^1/_4 \, ^1/_2 \, ^1/_2 \rangle$ modulations.[16,19] The soft Γ_{25} oxygen rotational modes have also been shown to provide the driving force from the high-temperature rhombohedral FE phase to the low-temperature FE phase.[29,30] We believe, in this case, that this is equivalent to the rhombohedral-FE-to-orthorhombic-PE morphotropic phase transition in the RE-doped BFO system.[8,14] The intensity of these superstructure reflections is very faint and this is an indication that these clusters exist at the nanoscale. Furthermore, the arrowed anomalous reflections next to the fundamental reflections are suggestive of possible structural deviations from the periodic lattice by oxygen octahedra, which seem to lead to a partially ordered structure.

The combined findings from Figures 1, 3, 4, and 5 reveal that, at $x = 0.1$, the A-site Sm dopant has a disrupted ideal perovskite network and induced structure deviations such as the formation of nanoscale clusters with antiparallel cation displacement along more than one orientational direction, as well as in-phase tilting of oxygen octahedra. Thus, Sm^{3+} doping seems to have destabilized the zone center FE polar state, concurrently promoting antipolar ordering by structural fluctuations that lead to the quadrupling of unit cell along many orientations, i.e., [011] and [$\bar{2}11$] directions along with slight distortion of the oxygen octahedral network.

Electron Energy-Loss Spectroscopy (EELS) Investigations. Single EEL spectra and line scans were collected from several regions with a superstructure (ordered region showing the quadrupling of the unit cell) and without a superstructure (aristotype region in the FE matrix) to identify the chemical environment responsible for the formation of antipolar clusters, as shown in Figure 6a, where the arrow gives the line scan direction. The recorded spectra were processed using the power-law background subtraction, and elemental ratios were quantified using Hartree−Slater cross sections.[31] Moreover, the near-edge structure (ELNES) of Fe L and O K edges was examined. Figures 6b−d show the comparison of the representative spectra from two regions of similar thickness with (red line) and without the superstructure (black line), normalized to the same integrated intensity for Fe, Sm, and O edge. Figure 6b shows the vicinity of the Fe L edge. The L_3 and L_2 lines are related to transitions of $2p^{3/2} \rightarrow 3d^{3/2} \, 3d^{5/2}$ and $2p^{1/2} \rightarrow 3d^{3/2}$, respectively, and their intensity ratio is dependent on the valence state.[32,33] We find that there is no statistically significant difference in the Fe L_3/L_2 intensity ratios between the regions with and without the

(24) Glazer, A. M. *Acta Crystallogr., Sect. A: Found Crystallogr.* **1975**, *A31*, 756.
(25) Woodward, P. M. *Acta Crystallogr., Sect. B: Struct. Sci.* **1997**, *B53*, 44.
(26) Marezio, M.; Remeika, J. P.; Dernier, P. D. *Acta Crystallogr., Sect. B: Struct. Crystallogr. Cryst. Chem.* **1970**, *B26*, 2008.
(27) Reaney, I. M.; Colla, E. L.; Setter, N. *Jpn. J. Appl. Phys.* **1994**, *33*, 3984.
(28) Glazer, A. M.; Ishida, K. *Ferroelectrics* **1974**, *6*, 219.

(29) Xu, Z.; Dai, X. H.; Li, J. F.; Viehland, D. *Appl. Phys. Lett.* **1995**, *66*, 2963.
(30) Dai, X. H.; Xu, Z. K.; Viehland, D. *J. Am. Ceram. Soc.* **1995**, *78*, 2815.
(31) Egerton, R. F. *Electron Energy-Loss Spectroscopy in the Electron Microscope*, 2nd Edition; Plenum Press: New York, 1996.
(32) Pearson, D. H.; Ahn, C. C.; Fultz, B. *Phys. Rev. B* **1993**, *47*, 8471.
(33) Pearson, D. H.; Fultz, B.; Ahn, C. C. *Appl. Phys. Lett.* **1988**, *53*, 1405.
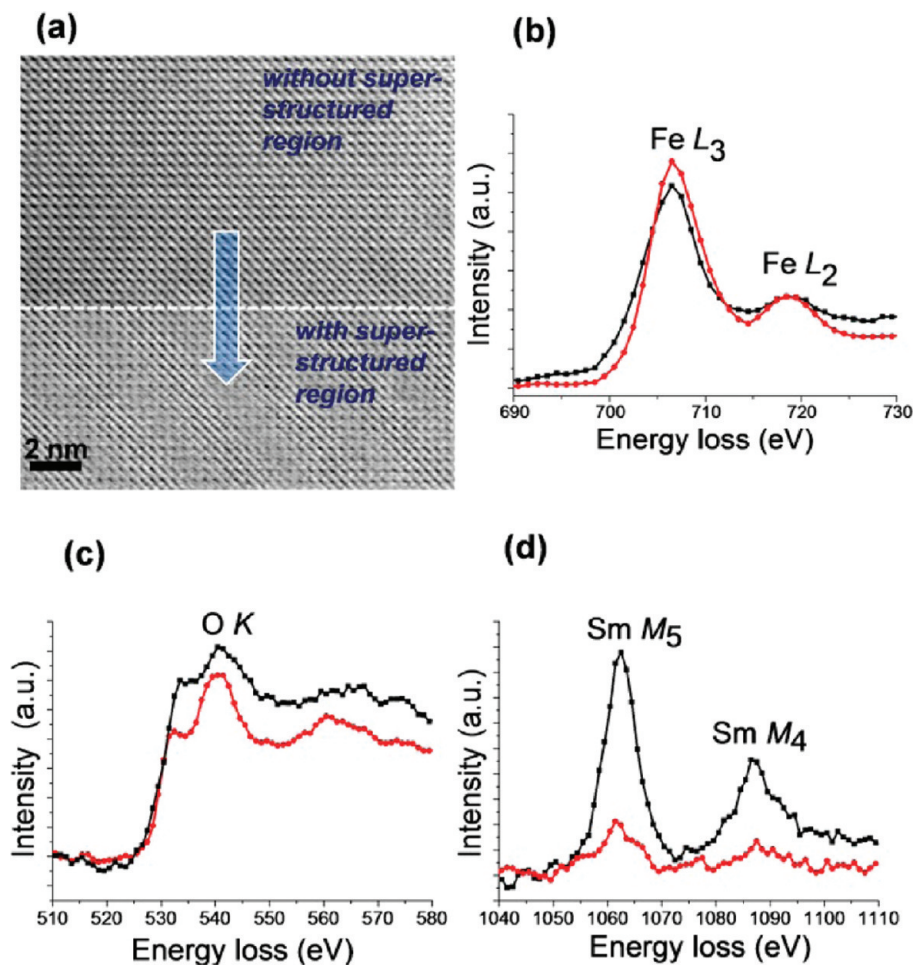
Figure 6. (a) [100] Zone axis cross-sectional STEM bright-field image with an arrow indicating the direction of the EELS line scan across regions with and without antipolar superstructures separated by the dashed lines; (b) Fe L edge spectra in the superstructure region (red line) and the region without the superstructure (black line); (c) O K edge spectra in the superstructure region (red line) and the region without the superstructure (black line); and (d) Sm M edge spectra in the superstructure region (red line) and the region without the superstructure (black line).

superstructure, thus indicating no change in the polar interaction between the Fe−O bond environment. Figure 6c shows the vicinity of the O K edge; the ELNES of this edge can be used to determine the density of unoccupied states.[34] Here also, no statistically significant change was observed. On the other hand, the integrated intensity of Sm M_5/M_4 edges seems to be significantly different for the regions with and without the superstructure (Figure 6d). In fact, the calculated Sm/Fe elemental ratio was 0.094 ± 0.007 for superstructure regions and 0.27 ± 0.08 for regions without the superstructure. For comparison, the O/Fe elemental ratio for the same spectra was 3.23 ± 0.33 and 2.94 ± 0.17, respectively.

The observed decrease in the intensity of the Sm edge is indeed surprising. We recall that these local antipolar pockets are observed only for compositions prior to the MPB (i.e., 14%-Sm-doped BFO).[10] We have shown that, for the MPB and cell-doubled orthorhombic phase compositions beyond the MPB, there is a distinct absence of any local structural inhomogeneities.[10] Therefore, we

preclude our thin-film synthesis procedure as the source of the local chemical inhomogeneity observed here. Furthermore, we do not observe any distribution of the lattice parameter; the XRD and electron diffraction patterns show very sharp well-defined peak positions. On the other hand, the results seen here reveal that the effect of the variation in samarium concentration for regions within and outside the pockets is more than merely a lattice distortion that one would expect from local inhomogeneities of doping concentration; it seems that this is an intrinsic process governed by local thermodynamics of the parent lattice in an effort to minimize local polar interactions. We are currently investigating the origin of the local variation in samarium concentration and its links to the concomitant distortion of the oxygen octahedral. Recently acquired near-edge X-ray absorption spectroscopy (NEXAFS) data indicates significant changes in the oxygen spectra as a function of samarium concentration. Perhaps the changes in the NEXAFS signature for the oxygen is an indication of the dramatic changes that the oxygen octahedral shell undergoes to accommodate the antiparallel shifts (created by introducing Sm). Thus, the local variations in Sm may be a reflection of the resistance of the parent

(34) Fuggle, J. C.; Inglesfield, J. E. *Unoccupied Electronic States: Fundamentals for XANES, EELS, IPS, and BIS*; Springer−Verlag: New York, 1992.
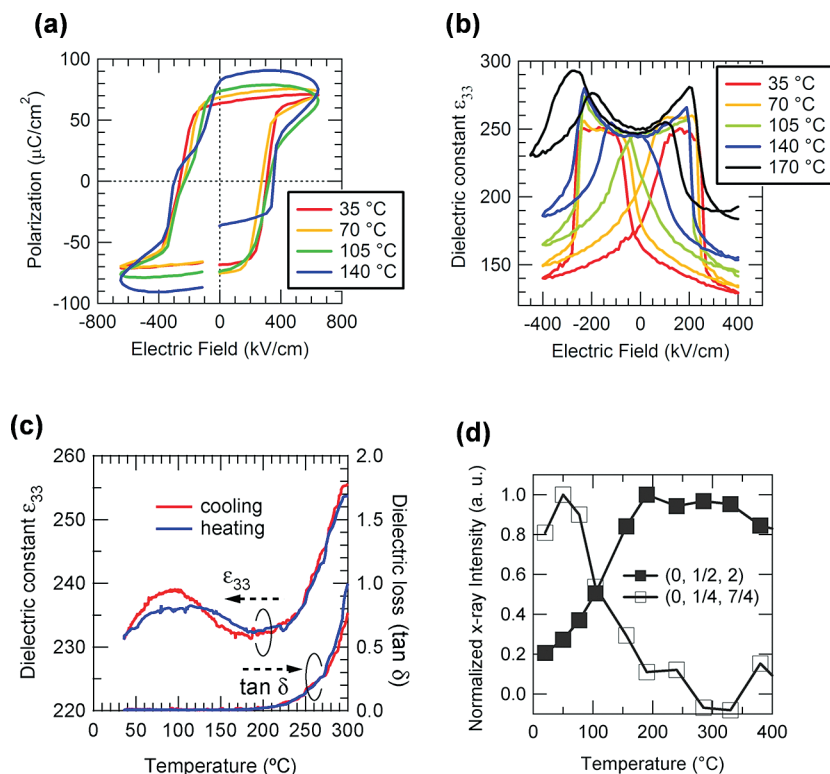
Figure 7. Temperature-dependent measurements were used to link macroscopic functional behavior and structural transitions in the $Bi_{0.9}Sm_{0.1}FeO_3$ thin film: (a) $P-E$ loops (25 kHz), showing FE to field-induced double hysteresis loops transition; (b) $\varepsilon_{33}-E$ loops indicating clear double-butterfly curves over 150 °C; (c) dielectric constant measurements (ε_{33}) and dielectric loss (tan δ), showing the effect of increased leakage current at higher temperatures upon heating and subsequent cooling; and (d) intensity of the (0, $^1/_4$, $^7/_4$) reflection (referred to as $^1/_4$) and the (0, $^1/_2$, 2) (referred to as $^1/_2$) reflection obtained from the XRD maps, as a function temperature. Notice the rapid reduction (increase) in the intensity for the $^1/_4$ ($^1/_2$) reflections with increasing temperature, implying that, at higher temperatures, the cell-doubled orthorhombic phase is more stable.

lattice to undergo long-range drastic changes in the bonding environments. Instead, by changing the samarium composition on a local scale, the lattice may have sought a compromise between the original FE lattice it prefers and the antiparallel cations imposed by the samarium doping. This is just our preliminary understanding ,and further detailed analysis will soon be reported.

Ferroelectric Property Measurements. To establish the link between stability of the antipolar ordered phase and its role on macroscopic properties, temperature-dependent electrical measurements must be investigated. Figures 7a, 7b, and 7c show the $P-E$ loop, $\varepsilon_{33}-E$ loop, and dielectric constant measurements, respectively, each as a function of temperature. The $P-E$ and $\varepsilon_{33}-E$ hysteresis loops have been reported (although in a different form) previously in ref 14. At room temperature, a square $P-E$ hysteresis curve can be seen, which indicates the presence of the dominant FE phase. Upon heating, a double hysteresis loop is observed for temperatures above and beyond 140 °C. Thus, while the local pockets show antipolar characteristics similar to PZO, the room-temperature FE loops still resemble that of a polar FE material. The double-hysteresis loop is understood to be the consequence of an electric-field-induced PE-to-FE phase transition.[14] It is interesting to note that spontaneous polarization does not vary much and retains a reasonably high polarization value, even at high temperatures. The FE to the double hysteresis loop transition is

clearer in the $\varepsilon_{33}-E$ curves shown in Figure 7b, which show distinct double "butterfly" curves over 150 °C. At temperatures of >250 °C, both dielectric constant (ε_{33}) and dielectric loss (tan δ) increase dramatically, indicating much increased leakage current (and loss) at higher temperatures. The ferroelectric and dielectric hysteresis data essentially reveal that, beyond a critical temperature, a regular FE order is suppressed and the field-induced double hysteretic behavior becomes favorable.[14]

Temperature-dependent 2D XRD maps were acquired for $Bi_{0.9}Sm_{0.1}FeO_3$ thin-film sample, as shown in Figure 7d, to link the observed functional behaviors in Figures 7a−(c) to a corresponding lattice structure. The result is summarized in Figure 7d, where the normalized intensities for the (0, $^1/_2$, 2) (referred to as $^1/_2$) and (0, $^1/_4$,$^7/_4$) (referred to as $^1/_4$) spots are plotted. There is a decrease in intensity of $^1/_4$ and an increase in intensity of $^1/_2$ superstructure reflections as the temperature is increased. The $^1/_4$ superstructures correspond to the family of $^1/_4${011} weak spots observed in the room-temperature electron diffraction patterns. Although high-temperature electron diffraction patterns are not presented in this study, from prior studies we are able to ascribe the (0, $^1/_2$, 2) spot to the presence of cell-doubled orthorhombic phase.[10] The presence of only the $^1/_2$ reflections at higher temperatures indicates that the orthorhombic cell-doubling phase is most stable at such temperature regimes. We have shown that, for the samarium-rich side of the

phase boundary, the $^1/_2$ superstructure reflections can be directly linked to the tilts of the oxygen octahedra. This has been recently corroborated in Nd-doped BFO as well, where the $^1/_4$ superstructure reflections have shown to disappear upon heating and the system undergoes a transformation from a PZO-like quadrupled cell to cell-doubled orthorhombic structure.[15] The $^1/_2$ superstructure reflections reach a maximum intensity at ~150 °C, which is in excellent agreement with the first change in shapes of dielectric loops and $P-E$ loops. The intensity curve, as a function of temperature, is gradual, where it can be deduced that the local interactions enforcing a change from quadrupling of the unit cells to doubling of unit cells is slow as the trivalent lanthanide dopant Sm^{3+} begins to control the phase stability.

Polar-to-antipolar phase transitions have been known to be diffuse as a function of temperature in a host of other systems, such as $BiNdFeO_3$,[11] $PbLaZrTiO_3$,[35] $NaNbO_3$,[36] and $SrCaTiO_3$.[37] The reduction in the intensity of the $^1/_4$ superstructure reflections with increasing temperature can be interpreted as a decrease in the amplitude of the cation displacements. Further details for this transition from the PZO-like clusters to a cell-doubled orthorhombic structure can be found elsewhere.[10] A similar trend has also been observed with BFO ceramics under hydrostatic compression, which undergo $R3c \rightarrow Pbam \rightarrow Pnma$ phase transitions.[38] In particular, it was found that BFO under a hydrostatic pressure of ~3 GPa has a structure related to the AFE PZO phase (space group *Pbam*).[38] Therefore, the RE substitution studied here apparently has an effect similar to that of applying pressure to the system. It shows that BFO is able to find the driving force for a morphotropic phase change under the influence of pressure either by solid-state chemistry routes via RE dopants[8,10] or external hydrostatic stress.[38]

IV. Conclusions

In conclusion, the local structure of antipolar clusters observed in a 10%-Sm^{3+}-doped BFO thin-film system has been investigated in detail. At room temperature,

HRTEM investigations show that Sm^{3+} doping has destabilized the zone-center ferroelectric (FE) polar state, resulting in zone-boundary antipolar clusters that show $^1/_4\{011\}$ superstructure reflections. The cations have antiparallel displacement along both the $[01\bar{1}]$ and $[11\bar{2}]$ directions, as well as in-phase octahedral tilts. Electron diffraction analyses revealed that, in these clusters, collective structure deviations away from the ideal aristotype structure play a fundamental role in the structure–property relationship. Aberration-corrected TEM imaging of the atomic displacements reveals the apparent antipolar order in this system is actually a lamellar array of highly dense ferroelectric domains with alternating polarizations. EEL spectra imply a valence state of Fe^{3+} which does not seem to vary much across the superstructure region, but it implies a possible shift in interaction between polar-to-antipolar order. Moreover, depletion of the Sm edge is found in the superstructure. X-ray diffraction (XRD) experiments, as a function of temperature, show that the intensity of $^1/_4$ reflections decreases with increasing temperature with a simultaneous increase in the intensity of $^1/_2$ superstructure spots. The $^1/_4$ reflections eventually die out, and the intensity of the $^1/_2$ reflections reaches a maximum at ~150 °C. This disappearance of the $^1/_4$ reflections and the consequent rise of the $^1/_2$ reflections is attributed to the previously reported rhombohedral ferroelectric to paraelectric cell-doubled orthorhombic phase transition.

Note Added after ASAP Publication. There was an error in caption of Figure 4 and a sentence about Figure 4 missing in the text in the version published ASAP February 26, 2010; the corrected version was published ASAP March 2, 2010.

Supporting Information Available: This material is available free of charge via the Internet at http://pubs.acs.org.

(35) Dai, X.; Xu, Z.; Viehland, D. *J. Appl. Phys.* **1996**, *79*, 1021.
(36) Lanfredi, S.; Lente, M. H.; Eiras, J. A. *Appl. Phys. Lett.* **2002**, *80*, 2731.
(37) Ranjan, R.; Pandey, D.; Lalla, N. P. *Phys. Rev. Lett.* **2000**, *84*, 3726.
(38) Belik, A. A.; Yusa, H.; Hirao, N.; Ohishi, Y.; Takayama-Muromachi, E. *Chem. Mater.* **2009**, *21*, 3400.